An investigation of the lowest-order transverse-electric (TE_1) mode of the parallel-plate waveguide for THz pulse propagation

Rajind Mendis and Daniel M. Mittleman**

Department of Electrical & Computer Engineering, Rice University, MS-366, 6100 Main Street, Houston, Texas 77005, USA
***Corresponding author: rajind@rice.edu*

Received February 2, 2009; accepted March 10, 2009;
posted March 30, 2009 (Doc. ID 107023); published April 27, 2009

We experimentally and theoretically investigate the lowest-order transverse-electric (TE_1) mode of the parallel-plate waveguide (PPWG) for the propagation of broadband THz pulses. We demonstrate undistorted THz pulse propagation via the single TE_1 mode, solving the group-velocity-dispersion and spectral-filtering problems caused by the mode's low-frequency cutoff. We observe a remarkable counterintuitive property of the TE_1 mode: its attenuation decreases with increasing frequency for all frequencies above cutoff. This phenomenon has not been observed with any other THz waveguide to date, and it can enable extremely low-loss propagation. We present a physical interpretation of this frequency-dependent behavior using a simple plane-wave description of the TE_1 mode propagation. We also find that it is possible to achieve almost 100% coupling to the TE_1 mode from a focused free-space Gaussian beam. In addition, using the above plane-wave analysis, we show how to mitigate the diffraction losses inherent to long path-length PPWGs via the use of transverse-concave plates.

OCIS codes: 230.7370, 320.5390, 320.5540.

1. INTRODUCTION

In recent years, numerous wave-guiding techniques have been investigated for the propagation of broadband THz pulses, using hollow metallic structures [1], dielectric fibers [2], dielectric slabs [3], parallel-plate structures [4,5], photonic crystal fibers [6], coaxial lines [7], metal wires [8–10], and metallic slits [11]. These have demonstrated great potential for applications such as high-speed interconnects, spectroscopy, sensing, imaging, microscopy, and signal processing. However, a THz wave-guiding technique that provides a complete solution, satisfying all of the requirements of low loss, low dispersion, single-mode propagation, with good energy confinement, and efficient input coupling, is still lacking. For example, the use of the dominant transverse-magnetic (TM_0) mode of a dielectric slab waveguide or the Sommerfeld mode of a cylindrical metal wire can provide extremely low intrinsic losses, but the former suffers from high group velocity dispersion (GVD) [3,12], while the latter is prone to radiation losses and suffers from poor coupling from a linearly polarized input beam [9,10]. Additionally, the use of the transverse-electromagnetic (TEM) mode of a parallel-plate waveguide (PPWG) can provide low losses, negligible dispersion, and very good coupling but cannot provide complete confinement, due to the one-dimensional nature of the guide [5].

Towards realizing the goal of a complete solution, we experimentally and theoretically investigate the lowest-order transverse-electric (TE_1) mode of the PPWG. This work is motivated by a series of studies performed in the mid-infrared in the 1970's [13–15]. These earlier studies have discussed the possibility of achieving extremely low losses (in the dB/km range) and good energy confinement via the use of the TE_1 mode, although under single-frequency or continuous-wave operation. However, until now, the TE_1 mode has not been considered for guiding THz pulses due to the obvious problems caused by the presence of a low-frequency cutoff $f_c=c/(2b)$, where b is the plate separation. For broadband THz pulses having frequency components extending from almost DC up to several THz, this would cause the loss of frequency components below cutoff and high GVD for components near the cutoff. These would result in severe distortion of the THz waveform and, therefore, have discouraged the use of this mode for THz pulse propagation in the past.

In this work, we show how to overcome these problems, and we demonstrate, for the first time to our knowledge, undistorted THz pulse propagation via the TE_1 mode. We also find that, (1) the mode attenuation resulting from ohmic losses actually decreases with increasing frequency for all frequencies above f_c—a phenomenon not observed with any other THz waveguide to date, and (2) one can achieve almost perfect input coupling to this mode from a linearly polarized free-space Gaussian beam. We additionally show how to achieve good *broadband* confinement via the use of transverse concave plates by resorting to a plane-wave analysis of the TE_1 mode propagation in the PPWG. These findings clearly demonstrate the very promising possibility of realizing a complete wave-guiding solution via the TE_1 mode.

2. EXPERIMENTAL DEMONSTRATION

For the experiment, we fabricate several PPWGs using highly polished aluminum plates, all having a transverse width larger than the ≈10 mm input-beam diameter. In the first set of measurements, the plates are spaced by $b=0.5$ mm. The THz pulses, generated and detected using a conventional terahertz–time-domain-spectroscopy (THz-TDS) system based on fiber-coupled photoconductive antennas, are coupled into and out of the PPWGs using two silicon plano-cylindrical lenses [3–5]. A typical input reference pulse is shown in Fig. 1(a), where the features seen after the main transient are inherent to the THz-TDS system. Its amplitude spectrum, derived by Fourier-transforming the truncated time domain signal, is shown in Fig. 2. Figure 1(b) shows the pulse after propagating through a 25.4 mm long PPWG, where the input Gaussian beam is polarized *parallel* to the plates to excite the TE_1 mode, in contrast to the more conventional excitation of the TEM mode where the input beam is polarized perpendicular to the plates [4,5]. This pulse is strongly reshaped and broadened to more than 150 ps, and it exhibits a notable positive chirp. Its amplitude spectrum (dotted curve in Fig. 2) exhibits a complete loss of spectral power up to $f_c=0.3$ THz, as expected for the TE_1 mode with $b=0.5$ mm. We conclude that the pulse propagates via the single TE_1 mode, as there are no visible interference effects in the time domain, and also because the next possible even-symmetric higher-order mode [1–5] (the TE_3 mode) has its cutoff at 0.9 THz, almost at the high-end of the input spectrum. Figure 1(c) shows the pulse after it propagates through a 6.4 mm long PPWG, again in the single-TE_1 mode. The shorter propagation length results in less broadening; but the positive chirp is still evident. The interference features that originate 43 ps after the main burst are due to round-trip reflections inside the waveguide. These were numerically removed in the subsequent analysis.

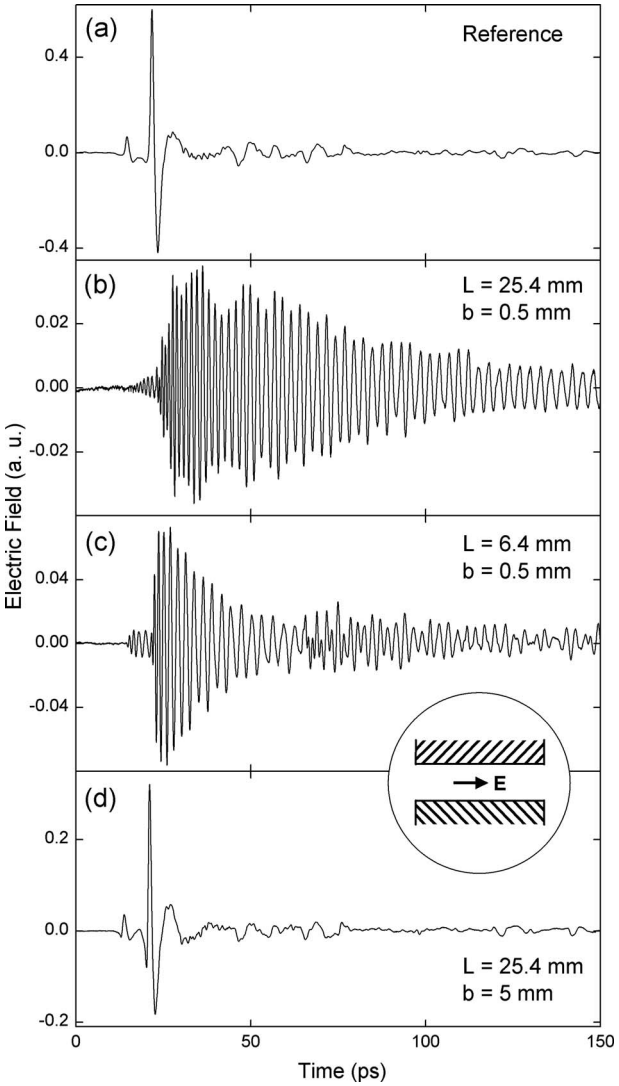

Fig. 1. Time-domain THz waveforms corresponding to (a) input reference, (b) TE_1-mode propagation in 25.4 mm long PPWG with $b=0.5$ mm, (c) TE_1-mode propagation in 6.4 mm long PPWG with $b=0.5$ mm, and (d) TE_1-mode propagation in 25.4 mm long PPWG with $b=5$ mm. The inset (circled) shows the excitation polarization axis with respect to the plate surfaces.

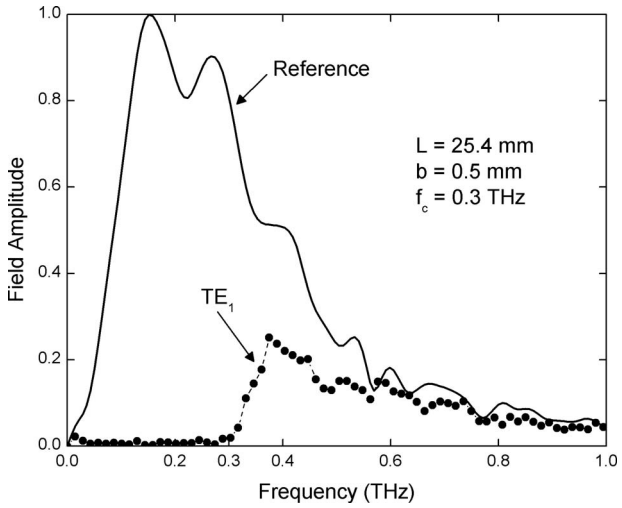

Fig. 2. Amplitude spectra corresponding to the scans in Figs. 1(a) and 1(b). The latter is given by the dots.

As in previous studies [4,5], by comparing the phase and amplitude spectra of the time signals in Figs. 1(b) and 1(c), we can extract the experimental phase constant β and attenuation constant α for the propagating mode. The derived phase velocity $v_p(=\omega/\beta)$ and group velocity $v_g(=\partial\omega/\partial\beta)$ are plotted in Fig. 3(a) by the open circles and dots, respectively. These show excellent agreement with the theoretical (thick solid) curves calculated using classical guided-wave theory [16,17] for the TE_1 mode of the PPWG with $b=0.5$ mm. The curves clearly demonstrate the highly dispersive nature of propagation due to the cutoff, where the high-frequency components travel faster, resulting in the observed positive chirp. The experimentally derived α is plotted in Fig. 4(a) by the dots, along with the corresponding theoretical (thick solid) curve, computed using the expression [16]

$$\alpha = \frac{4R_s(f_c/f)^2}{Z_o b\sqrt{1-(f_c/f)^2}}. \quad (1)$$

Here, Z_o is the free-space impedance and R_s is the surface resistance of the metal plates given by $R_s=\sqrt{\pi f\mu/\sigma}$, where μ is the permeability and σ is the DC conductivity. The

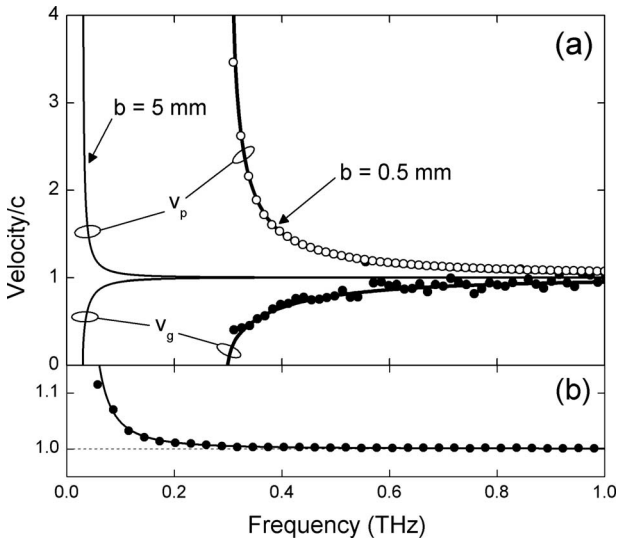

Fig. 3. (a) Phase and group velocity for the TE_1 mode. The theoretical thick and thin solid curves are for $b=0.5$ mm and 5 mm, respectively. The open circles and dots are experimental. (b) Close-up of the phase velocity for $b=5$ mm. The solid curve is theoretical and the dots are experimental.

experimental and theoretical curves agree reasonably well, and they reveal a remarkable counterintuitive property of the TE_1 mode: the attenuation *decreases* with increasing frequency for *all frequencies above cutoff*. This type of dependence has not been observed with any other THz waveguide [1–11,18]. It is important to note that this characteristic behavior is true for all frequencies above cutoff, and is truly a unique observation, distinct from previous THz studies, for example, on hollow-core waveguides [1,18], where the attenuation decreases for frequencies immediately above the cutoff but then increases for even higher frequencies. As discussed in Section 3 below, we can gain some physical insight into this behavior via a *bouncing-plane-wave* description of the TE_1 mode propagation.

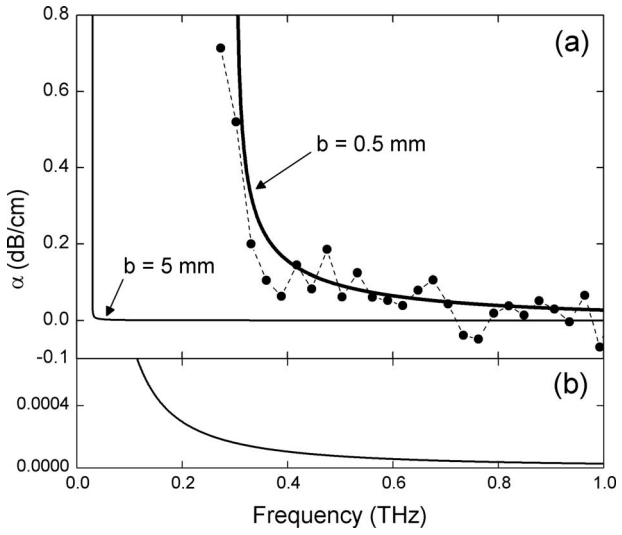

Fig. 4. (a) The attenuation constant for the TE_1 mode. The theoretical thick and thin solid curves are for $b=0.5$ mm and 5 mm, respectively. The dots are experimental. (b) Close-up of the baseline of the theoretical curve for $b=5$ mm.

The significance of this frequency dependence is that it allows one to reduce the attenuation by pushing f_c to lower frequencies. We can lower f_c by increasing the plate separation. For example, when $b=5$ mm, $f_c=30$ GHz, which is at the low end of the input spectrum for our pulses (see Fig. 2). The corresponding theoretical attenuation is also plotted in Fig. 4(a) (thin solid curve), with an enlarged view of the baseline shown in Fig. 4(b). This indicates that an extraordinarily low attenuation is attainable. For example, the value at 1 THz is 2.6 dB/km, only an order of magnitude higher than the attenuation of telecommunications-grade optical fiber at $\lambda=1550$ nm. Furthermore, lowering f_c also helps to maintain the spectral integrity of the input pulses, while reducing the GVD to almost negligible values, as seen by the (thin solid) velocity curves plotted in Fig. 3(a) for $b=5$ mm. Except for the very low end of the spectrum, the curves exhibits almost zero dispersion.

The idea of shifting f_c to the low-frequency end by increasing the plate separation has not been explored previously for the PPWG, but a similar concept has been studied for the transport of microwave radiation in a hollow metallic circular waveguide, in the 1970's [19]. In that case, as in our situation, one encounters the obvious disadvantage of permitting multimode propagation, resulting in an *over-moded* waveguide. Since the cutoff frequencies of many higher-order modes now fall within the input spectrum, multiple modes could be simultaneously excited, leading to excessive loss, dispersion, and mode conversion. For example, when $b=5$ mm, there exist 17 possible even-symmetric TE modes (TE_1, TE_3, TE_5, TE_7, ….., and TE_{33}) having cutoff frequencies that lie within our input spectrum. However, similar to the earlier study [19], this problem can be overcome if the input coupling is optimized to selectively excite only the TE_1 mode via mode matching. In fact, the electric field of the TE_1 mode has a spatial dependence of $E(y)\sim\sin(\pi y/b)$, where y is the coordinate normal to the plates with the origin at the plate surface. This spatial profile is well matched to a Gaussian input beam and should, therefore, enable better coupling than can be achieved with the more commonly used TEM mode, which has a flat spatial profile. To quantify this, we calculate the power coupling efficiency (η) from an input Gaussian beam to several lower-order even-symmetric TE modes, as a function of b/D, where D is the $1/e$ beam size of the Gaussian at the input face of the waveguide. This result, plotted in Fig. 5, shows that the maximum possible η to the TE_1 mode is 99%, achieved when $b/D=1.42$. In fact, $\eta>90\%$ for the TE_1 mode when $0.53<b/D<2.1$, implying that we can achieve almost purely single-TE_1 mode excitation for a large range of input beam sizes.

With the above understanding, we have the freedom to select a practically feasible, large value for b to achieve extremely low losses and negligible pulse distortion, while selecting a matching input beam size to couple all of the available power to the single TE_1 mode. In an attempt to test some of these capabilities, as a first demonstration, we use the same PPWGs as in our earlier measurements, but with a large plate separation, $b=5$ mm. We directly excite the guided wave with a weakly focused THz input beam, without using cylindrical lenses. Figure 1(d) shows the resulting pulse after propagation through a 25.4 mm

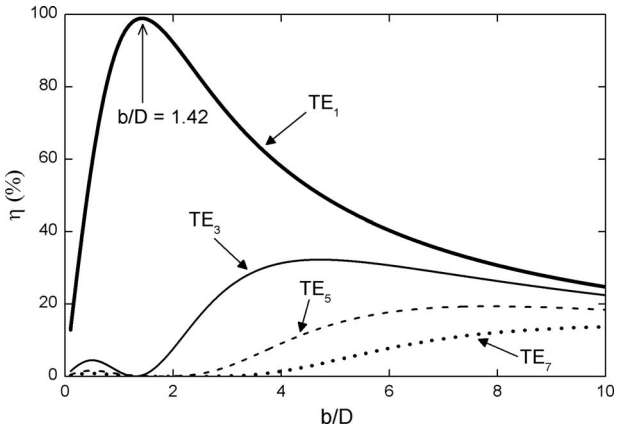

Fig. 5. The power-coupling efficiency from an input Gaussian beam to several even-symmetric TE modes of the PPWG.

long PPWG. We observe only a minor reshaping of the pulse, in sharp contrast to the severe pulse distortion seen in Figs. 1(b) and 1(c). The experimentally derived phase velocity for this larger value of b, shown in Fig. 3(b) by the dots, is in excellent agreement with the theoretical prediction shown by the solid curve, indicating almost negligible dispersion. This clearly demonstrates that we have achieved single TE_1 mode propagation, implying the high selectivity of the input coupling, and moreover, it demonstrates that we have successfully overcome the problems associated with the cutoff.

Although we expect the attenuation of the pulses propagating in these PPWGs to be extremely low, as predicted in Fig. 4(b), an experimental determination of this parameter is not possible here, because the losses are far too small to measure with these propagation lengths. However, if we were to employ longer path lengths, we would encounter the problem of energy leakage caused by wave diffraction in the unconfined (transverse) direction [5]. Since the ohmic attenuation would be extremely small, this diffraction loss would be expected to be the dominant loss mechanism in long waveguides. Therefore, it is important to control this diffraction loss to achieve good confinement behavior when practically utilizing this wave-guiding technique for long-distance transmission. In order to achieve this, we turn to a previously proposed idea of using transverse concave plates [13,15]. It has been demonstrated that concave plates having a slight curvature can provide the necessary confinement at a single frequency ($\lambda = 10.6\ \mu$m) [13]. In our case, where we are dealing with pulses, we have to investigate the feasibility of this method for a *broadband* THz spectrum, and this is discussed in Section 4 below.

The following sections are theoretical analyses, where in Section 3, we present a bouncing-plane-wave description of the propagating modes in a PPWG, starting from generalized TE modes, and then, derive the attenuation for the TE_1 mode based on this simple plane-wave picture and compare to that given by Eq. (1). This is followed by a physical interpretation of the characteristic frequency dependence of the attenuation observed in our experimental work, where the discussion is extended to include the TM modes of the PPWG. Specifically, we compare the attenuation behavior of the TE_1 mode to that of the TM_1 mode, and also to the well-known attenuation of the TE_{10} mode of a hollow, metallic rectangular waveguide [1,16,17] that is widely used for the transport of microwave radiation. Finally, in Section 4, we use this plane-wave picture to analyze the diffraction losses for the TE_1 mode in a long waveguide, and show how this could be controlled via the use of transverse concave plates to achieve complete confinement.

3. WAVEGUIDE LOSS CALCULATIONS

Based on the well-known classical guided-wave theory [16], for an input electric field that is linearly polarized in a direction (x) parallel to the plane of the plates, only TE_n modes can exist in the PPWG. With plates made of perfect electric conductors, separated by air, the nonvanishing terms of the modal field components for z-directed propagation are

$$E_x = \frac{A_n \beta_y}{\varepsilon_o} \sin(\beta_y y) e^{-j\beta_z z}, \tag{2}$$

$$H_y = \frac{A_n \beta_y \beta_z}{\omega \mu_o \varepsilon_o} \sin(\beta_y y) e^{-j\beta_z z}, \tag{3}$$

$$H_z = -\frac{jA_n \beta_y^2}{\omega \mu_o \varepsilon_o} \cos(\beta_y y) e^{-j\beta_z z}, \tag{4}$$

where $\beta_y = n\pi/b$ with $n = 1, 2, 3, \ldots$. In these expressions, ω, μ_0, ε_0, β have their usual meanings, the constant A_n depends on the input excitation of the PPWG, and subscripts x, y, z indicate the respective spatial directions as designated in Fig. 6.

By converting the sinusoidal functions in Eqs. (2)–(4) to exponentials, we can represent the field components as superpositions of upward and downward traveling plane waves of the form

$$E_x, H_y, H_z \propto (e^{-j\beta_y y} \mp e^{+j\beta_y y}) e^{-j\beta_z z}. \tag{5}$$

This implies that the TE-mode propagation in the PPWG is equivalent to two plane waves bouncing back and forth between the plates with s-polarized incidence while moving in the z direction. Without loss of generality, we will use only one plane wave for the following discussion as depicted in Fig. 6, whose phase constant $\beta_0 = \sqrt{\beta_y^2 + \beta_z^2} = 2\pi/\lambda_0$.

Taking into consideration the y component of the phase constant, we can write $\beta_0 \cos\theta = \beta_y$, which gives the angle of incidence of the plane wave at the metal surface as

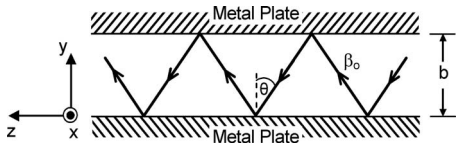

Fig. 6. Longitudinal cross section of the PPWG depicting the bouncing plane wave.

$$\theta = \cos^{-1}\left(\frac{\beta_y}{\beta_o}\right) = \cos^{-1}\left(\frac{n\lambda_o}{2b}\right). \quad (6)$$

Here, $n\lambda_0/(2b) \leq 1$, defines the cutoff condition for the TE modes of the waveguide, and results in the cutoff frequency $f_c = nc/(2b)$. According to Eq. (6), for a given plate separation, when the frequency goes down, the angle θ associated with any TE_n mode also goes down, and at cutoff is equal to zero (i.e., normal incidence). Correspondingly, when the frequency goes up, θ gets closer to 90°, where the plane wave approaches grazing incidence. This frequency dependence is shown in Fig. 7 for the TE_1 mode with $b = 0.5$ mm, where the cutoff frequency $f_c = 0.3$ THz is indicated by the dashed line. We note that this general dependence is common to all the TE_n modes, where the relative differences among the modes arise in the form of a smaller θ for a particular frequency as the order n of the mode becomes higher.

For a given waveguide length, as θ varies with frequency, the number of bounces N of the plane wave will also vary with the frequency, where N increases as the frequency decreases. By dividing the waveguide length by the spacing required for one bounce, we can calculate

$$N = \frac{1}{b}\cot\theta, \quad (7)$$

for a waveguide length of one meter. The frequency dependence of N is also plotted in Fig. 7 for the TE_1 mode with $b = 0.5$ mm. We note that the number of bounces increase asymptotically at the cutoff frequency, at which point the plane wave simply bounces vertically up and down without moving in the z direction.

In order to derive the attenuation of a practical waveguide where the plates are not made of perfect electric conductors, we can use the above plane-wave description of the modes and calculate the losses due to the bounces occurring at the plate surfaces. At each bounce there will be some power loss due to the imperfectly conducting surfaces, which can be deduced by considering the Fresnel reflection coefficient at the air–metal boundary under oblique incidence of the plane wave.

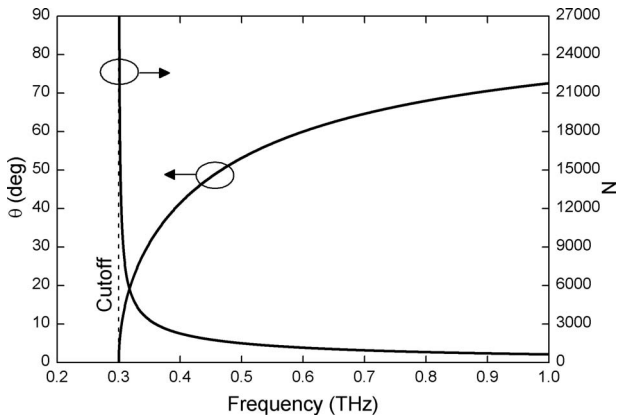

Fig. 7. Frequency dependence of the incidence angle θ [left vertical axis] and the number of bounces N per meter length of the waveguide [right vertical axis], for the plane wave corresponding to the TE_1 mode with $b = 0.5$ mm. The cutoff frequency is indicated by the dashed line.

The reflection coefficient r_s for s-polarized incidence is given by the well-known expression [17]

$$r_s = \frac{Z_2\cos\theta_i - Z_1\cos\theta_t}{Z_2\cos\theta_i + Z_1\cos\theta_t}, \quad (8)$$

where Z_1 and Z_2 are the intrinsic impedances of the media on either side of the boundary, subscript 1 denoting the incidence side, and θ_i and θ_t are the angles of incidence and transmission, respectively. For the air–metal boundary in Fig. 6, $\theta_i = \theta$, and it can be shown that $\theta_t = 0°$ always, due to the high conductivity of the metallic media.

Starting from the general expression $Z = \sqrt{j\omega\mu/(\sigma + j\omega\varepsilon)}$ for the intrinsic impedance of a medium, where the conductivity σ accounts for any losses, we can obtain the impedance ratio for the air and metallic media as

$$\frac{Z_1}{Z_2} \approx \sqrt{\frac{\sigma}{j\omega\varepsilon_o}}, \quad (9)$$

where the approximation holds under the high conductivity of the metal. In the following analysis, we assume σ to be equal to its DC value, since aluminum, used to fabricate the PPWGs in our experimental work, has a flat response in our frequency range. Substituting the impedance ratio from Eq. (9), and θ from Eq. (6), into Eq. (8), we can calculate r_s as a function of frequency, whose magnitude is plotted (upper curve) in Fig. 8. This curve indicates a very mild frequency dependence, slowly increasing with increasing frequency. For comparison, we have also plotted in the same figure, the magnitude of the reflection coefficient r_p under p-polarized incidence. This shows a much stronger dependence with frequency, and more strikingly, the opposite dependence, decreasing with increasing frequency. The significance of these opposing frequency dependences will be apparent later.

We can now derive the attenuation constant α, which is defined as the power loss per unit length, by taking the product of the number of bounces per unit length and the power loss per bounce. For a unit power, the power loss per bounce is equal to $(1 - |r_s|^2)$. Therefore,

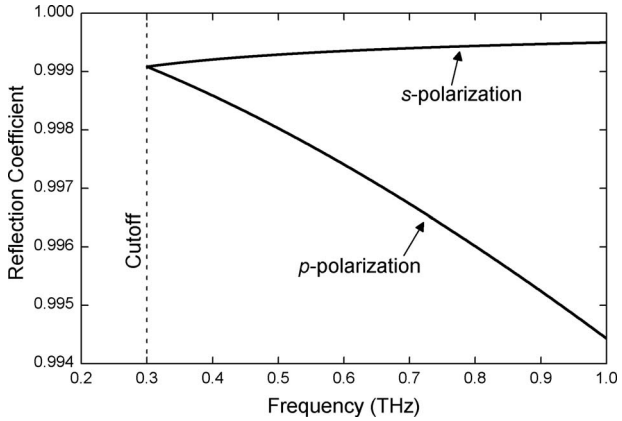

Fig. 8. Magnitude of the reflection coefficient for the plane-wave incident at the air–metal boundary for the two orthogonal polarizations s and p, which correspond to the TE_1 and TM_1 modes, respectively. The conductivity of the metal is taken to be 3.96×10^7 S/m, the DC conductivity of aluminum.

$$\alpha = N(1 - |r_s|^2). \quad (10)$$

This quantity is plotted in Fig. 9 by the dots, along with that computed using Eq. (1) by the solid curve. The agreement is so good that the two curves are *indistinguishable* at this scale. This comparison not only strengthens the validity of the plane-wave argument, but also proves the mathematical accuracy of Eq. (1), which is stated in [16] without any proof. These curves clearly indicate the counterintuitive frequency dependence observed in our work, where the TE_1 mode attenuation decreases with increasing frequency for all frequencies above cutoff.

We can compare this loss behavior to that of TM modes of the PPWG, by resorting to the same plane-wave description to derive the attenuation constant, but in this case, with *p*-polarized incidence. We note that the lowest-order TM mode, which is the TEM mode, cannot be analyzed using this bouncing-plane-wave picture, since the associated plane wave undergoes no bounces but propagates at grazing incidence at the metal surfaces at all frequencies. For all other TM modes, the plane-wave description will be valid and analogous to the TE modes, except that the reflection is *p* polarized rather than *s* polarized. The resulting TM_1 mode attenuation is also plotted in Fig. 9 by the squares, using the r_p values in Fig. 8, along with that corresponding to the loss expression given in [16] by the solid curve. Again we see excellent agreement between the two curves, but this time with a different frequency dependence compared to that of the TE_1 mode. In fact, this is the characteristic frequency dependence that one would encounter in a hollow metallic rectangular waveguide—the attenuation decreases sharply near the cutoff, and then it increases when moving away from cutoff as the frequency increases [1,16,17].

Now that we have a very simple way to understand the loss behavior, it is possible to gain some physical insight into the origin of the frequency dependence in the TE_1 mode. Since the number of bounces of the plane wave follows the same dependence for both the TE_1 and TM_1 modes, the discrepancy in the frequency dependence is directly related to the reflection coefficient. If the magnitude of the reflection coefficient remained constant with frequency, the variation in the number of bounces would cause the loss to decrease monotonically with frequency. Since the magnitude increases (although slightly) in the TE_1 case, this assists to pull the loss down even more with frequency, whereas, since the magnitude decreases (relatively strongly) in the TM_1 case, this will tend to pull the loss up as the frequency increases. Therefore, this plane-wave picture clearly explains the contrasting difference in the loss behavior of the TE_1 mode compared to the TM_1 mode. We conclude that the characteristic frequency dependence in the TE_1 mode's attenuation is dominated by the frequency dependence of the number of bounces, and not so much by the ohmic loss (at each bounce), resolving the counterintuitive aspect of this behavior.

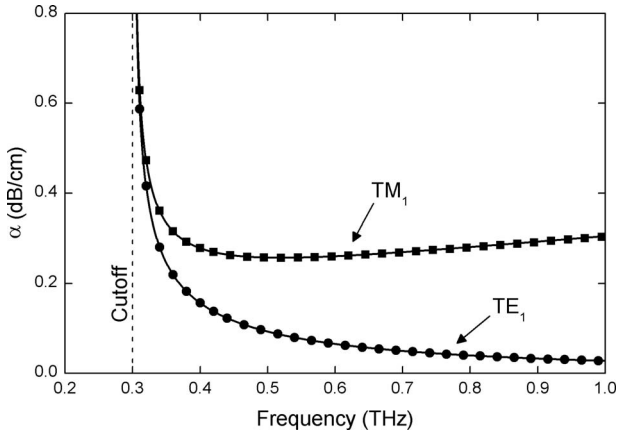

Fig. 9. Comparison of the attenuation constant derived using the simple plane-wave description and the expressions given in [16]. The derived curves are represented by the dots and squares for the TE_1 and TM_1 modes, respectively, whereas the solid curves are from [16]. The agreement is so good that the corresponding curves are *indistinguishable* at this scale. The unique frequency dependence of decreasing attenuation for all frequencies above cutoff for the TE_1 mode, in contrast to that of the TM_1 mode, is clearly evident.

Interestingly, we can extend this plane-wave description to the dominant TE_{10} mode of the hollow metallic rectangular waveguide. We can show that the TE_{10}-mode propagation can be described by two plane waves bouncing back and forth, with *s*-polarized incidence, between the plates making up the long sides of the rectangular cross section. Therefore, as far as the bouncing plane wave is concerned, it is similar to the TE_1 situation of the PPWG. However, there is one major difference in that the plane wave simultaneously undergoes grazing incidence in a *p*-polarized sense at the plates making up the short sides. Therefore we can expect that, while the *s*-polarized plane-wave contribution could assist to bring down the loss as the frequency increases, similar to the TE_1 case, the *p*-polarized part of the contribution would tend to bring it up with frequency, resulting in the well-known frequency dependence of a sharp decrease near the cutoff and a steady increase away from cutoff [1,16,17].

4. LOSSES DUE TO DIFFRACTION

An added advantage of the plane-wave description of the modes is that it provides a convenient way to analyze the spatial extent of the beam in the unconfined *x* direction of the waveguide and thereby look at possible ways to mitigate any losses that may arise due to beam diffraction. This is an important consideration in the practical implementation of a long-path-length PPWG. As we would normally couple energy to the waveguide using a Gaussian beam, it is reasonable to expect the plane wave to diffract in the unconfined dimension, according to Gaussian beam optics. Based on this intuitive picture, it is easy to visualize that, by introducing a slight curvature to the plate surfaces (a transverse concavity), we could, in principle, negate the diffraction by imparting a slight focusing effect at each bounce of the wave [13,15]. Incidentally, although we could expect this idea to work for the TE_1 mode, it would not be expected to work for the TEM mode, since the associated plane wave undergoes no bounces.

The cross-sectional geometry of this modified plate configuration is illustrated in Fig. 10(a), where the inner surfaces exhibit a cylindrical curvature with a radius R. This curvature will impart a lateral focusing effect to the beam as it bounces off the surface, similar to a plano-concave

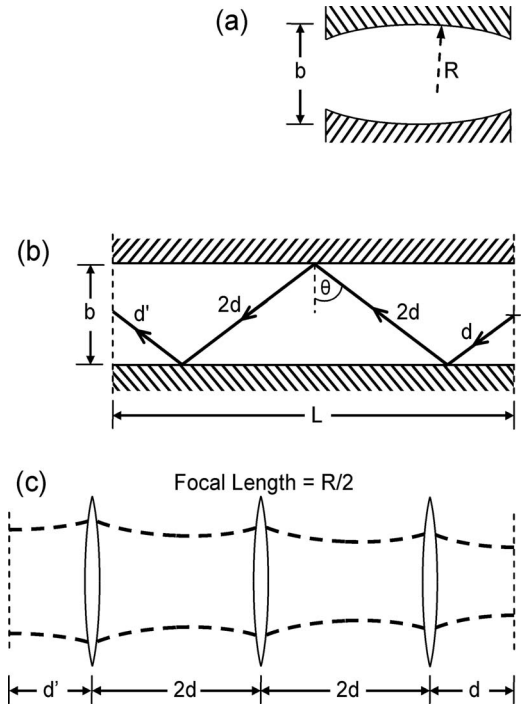

Fig. 10. (a) Transverse cross section of the PPWG showing the concave plate geometry. (b) Longitudinal cross section of the PPWG, indicating the path of the associated plane wave for the case of three bounces within the length L. (c) The equivalent unfolded lateral beam profile of the bouncing wave, where the thin lenses simulate the focusing effect caused by the curvature.

mirror with a focal length of $R/2$. We resort to Gaussian beam optics to derive the lateral divergence of the beam and, for simplicity, assume that the wave originates centered at the input plane of the PPWG as shown in Fig. 10(b). This diagram illustrates a particular situation when the wave undergoes three bounces as it propagates from the input to the output, where the bounce-to-bounce propagation distance is $2d$. It is important to note that the actual propagation distance for the bouncing wave is longer than the length L of the PPWG; in this case, it is equal to $5d+d'$, where d' is the final path-length segment after the last bounce. Figure 10(c) illustrates the lateral profile of the "unfolded" propagating wave, where the repetitive interaction with the curved surface is simulated by a series of identical thin lenses with focal length $R/2$. For this optical configuration, we can write a generalized expression for the ABCD matrix [20] as

$$\begin{bmatrix} A & B \\ C & D \end{bmatrix} = \begin{bmatrix} 1 & d' \\ 0 & 1 \end{bmatrix} \left[\begin{bmatrix} 1 & 0 \\ -2/R & 1 \end{bmatrix} \begin{bmatrix} 1 & 2d \\ 0 & 1 \end{bmatrix} \right]^{(N-1)} \begin{bmatrix} 1 & 0 \\ -2/R & 1 \end{bmatrix} \times \begin{bmatrix} 1 & d \\ 0 & 1 \end{bmatrix}, \tag{11}$$

where $d' = (L/\sin\theta) - d(2N-1)$, and the number of bounces $N > 0$. In the trivial case of no bounces, the expression reduces to only the first matrix with $d' = L/\sin\theta$.

We apply this theoretical formalism to a 1 m long PPWG having a plate separation of 10 mm, starting from a frequency-independent lateral $1/e$ beam size of 2 cm at the input plane. Figure 11 shows the computed lateral $1/e$ beam size at the output plane of the PPWG as a function

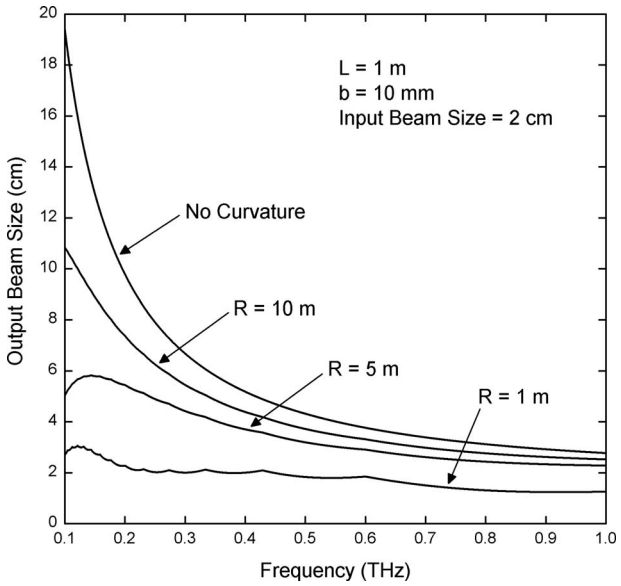

Fig. 11. Lateral beam size at the output of the PPWG as a function of frequency for varying radii of curvature of the plates.

of the frequency, for several different values of the curvature ranging from no-curvature (flat plates) to $R = 1$ m. For the flat plates, the beam size increases as the frequency decreases due to diffraction, reaching an impractical size of 20 cm at a frequency of 0.1 THz at the output. In a real-world situation, where the plates need to have a finite width, it is clear that this low-frequency energy would leak out of the PPWG giving rise to the aforementioned diffraction loss. However, as we increase the curvature (reduce R), we note that the output beam size is gradually reduced, with a proportionally higher reduction occurring at the low frequencies. When $R = 1$ m, the beam size is relatively close to the input size of 2 cm throughout the spectrum, allowing one to extract all the energy at the output. The reason for this frequency-dependent reduction in beam size is the varying number of bounces as the frequency changes. Interestingly, low-frequency waves undergo more bounces (as shown earlier), which assists to accumulate a higher degree of focusing, thereby naturally providing the required relative-frequency dependent effect to mitigate the diffraction problem in a *broadband* sense. Furthermore, the curves in Fig. 11 indicate a characteristic segmented nature, implying different operating regimes in different spectral regions. This is a consequence of the number of bounces varying in a discrete manner with frequency, when moving from one operating regime to the next.

5. CONCLUSIONS

We have demonstrated how to achieve undistorted THz pulse propagation via the single TE_1 mode of the PPWG, overcoming the GVD and spectral-filtering problems caused by the mode's low frequency cutoff. We experimentally achieve this using an over-moded PPWG, where the spectral bandwidth of the input THz pulses span 17 possible waveguide modes. Single-mode propagation is made possible by the almost perfect TE_1-mode selectivity by the

input Gaussian beam. We observe that the mode's ohmic attenuation decreases with increasing frequency, a counterintuitive property that would enable extremely low-loss propagation, and we explain this behavior using a simple bouncing-plane-wave analysis. We theoretically demonstrate that the use of transverse concave plates can provide the necessary complete confinement for long-path-length PPWGs. These findings open up the possibility of realizing a complete THz wave-guiding solution via the use of the TE_1 mode of the PPWG, which would provide low loss, low dispersion single-mode propagation with good energy confinement and efficient input coupling.

ACKNOWLEDGMENTS

This work was supported in part by the National Science Foundation (NSF) and by the United States Air Force Research Laboratory.

REFERENCES

1. G. Gallot, S. P. Jamison, R. W. McGowan, and D. Grischkowsky, "Terahertz waveguides," J. Opt. Soc. Am. B **17**, 851–863 (2000).
2. S. P. Jamison, R. W. McGowan, and D. Grischkowsky, "Single-mode waveguide propagation and reshaping of sub-ps terahertz pulses in sapphire fibers," Appl. Phys. Lett. **76**, 1987–1989 (2000).
3. R. Mendis and D. Grischkowsky, "Plastic ribbon THz waveguide," J. Appl. Phys. **88**, 4449–4451 (2001).
4. R. Mendis and D. Grischkowsky, "Undistorted guided-wave propagation of subpicosecond terahertz pulses," Opt. Lett. **26**, 846–848 (2001).
5. R. Mendis and D. Gischkowsky, "THz interconnect with low loss and low group velocity dispersion," IEEE Microw. Wirel. Compon. Lett. **11**, 444–446 (2001).
6. H. Han, H. Park, M. Cho, and J. Kim, "Terahertz pulse propagation in a plastic photonic crystal fiber," Appl. Phys. Lett. **80**, 2634–2636 (2002).
7. T. -I. Jeon and D. Grischkowsky, "Direct optoelectronic generation and detection of sub-ps electrical pulses on sub-mm coaxial transmission lines," Appl. Phys. Lett. **85**, 6092–6094 (2004).
8. K. Wang and D. M. Mittleman, "Metal wires for terahertz wave guiding," Nature **432**, 376–379 (2004).
9. T. -I. Jeon, J. Zhang, and D. Grischkowsky, "THz Sommerfeld wave propagation on a single metal wire," Appl. Phys. Lett. **86**, 161904 (2005).
10. K. Wang and D. M. Mittleman, "Guided propagation of terahertz pulses on metal wires," J. Opt. Soc. Am. B **22**, 2001–2008 (2005).
11. M. Wachter, M. Nagel, and H. Kurz, "Metallic slit waveguide for dispersion-free low-loss terahertz signal transmission," Appl. Phys. Lett. **90**, 061111 (2007).
12. R. Mendis, "Comment on "Low-loss terahertz ribbon waveguides"," Appl. Opt. **47**, 4231–4234 (2008).
13. H. Nishihara, T. Inoue, and J. Koyama, "Low-loss parallel-plate waveguide at 10.6 μm," Appl. Phys. Lett. **25**, 391–393 (1974).
14. E. Garmire, T. McMahon, and M. Bass, "Flexible infrared-transmissive metal waveguides," Appl. Phys. Lett. **29**, 254–256 (1976).
15. Y. Mizushima, T. Sugeta, T. Urisu, H. Nishihara, and J. Koyama, "Ultralow loss waveguide for long distance transmission," Appl. Opt. **19**, 3259–3260 (1980).
16. N. Marcuvitz, *Waveguide Handbook* (Peregrinus, 1993).
17. C. A. Balanis, *Advanced Engineering Electromagnetics* (Wiley, 1989).
18. Y. Jiang, C. Jing, W. A. Peebles, D. L. Brower, and J. L. Doane, "Improved performance of an optically pumped FIR laser using metallic waveguide," Rev. Sci. Instrum. **63**, 4672–4674 (1992).
19. T. A. Abele, D. A. Alsberg, and P. T. Hutchison, "A high-capacity digital communication system using TE_{01} transmission in circular waveguide," IEEE Trans. Microwave Theory Tech. **23**, 326–333 (1975).
20. J. T. Verdeyen, *Laser Electronics* (Prentice Hall, 1995).